Search for tetraquark states $X_{cc\bar{s}\bar{s}}$ in $D_s^+ D_s^+$ ($D_s^{*+} D_s^{*+}$) final states at Belle

X. Y. Gao,[13] Y. Li,[13] C. P. Shen,[13] I. Adachi,[21,17] H. Aihara,[90] D. M. Asner,[3] H. Atmacan,[8] T. Aushev,[23] R. Ayad,[84] P. Behera,[29] K. Belous,[33] M. Bessner,[20] V. Bhardwaj,[26] B. Bhuyan,[27] T. Bilka,[5] A. Bobrov,[4,69] D. Bodrov,[23,47] G. Bonvicini,[94] J. Borah,[27] A. Bozek,[65] M. Bračko,[53,39] T. E. Browder,[20] A. Budano,[35] M. Campajola,[34,61] D. Červenkov,[5] M.-C. Chang,[12] P. Chang,[64] A. Chen,[63] B. G. Cheon,[19] K. Chilikin,[47] H. E. Cho,[19] K. Cho,[43] S.-J. Cho,[96] S.-K. Choi,[7] Y. Choi,[82] S. Choudhury,[37] D. Cinabro,[94] S. Cunliffe,[9] S. Das,[52] G. De Pietro,[35] R. Dhamija,[28] F. Di Capua,[34,61] J. Dingfelder,[2] Z. Doležal,[5] T. V. Dong,[11] D. Dossett,[55] D. Epifanov,[4,69] T. Ferber,[9] A. Frey,[16] B. G. Fulsom,[71] R. Garg,[72] V. Gaur,[93] N. Gabyshev,[4,69] A. Giri,[28] P. Goldenzweig,[40] T. Gu,[73] Y. Guan,[8] K. Gudkova,[4,69] C. Hadjivasiliou,[71] S. Halder,[85] O. Hartbrich,[20] K. Hayasaka,[67] H. Hayashii,[62] M. T. Hedges,[20] W.-S. Hou,[64] C.-L. Hsu,[83] T. Iijima,[60,59] K. Inami,[59] G. Inguglia,[32] A. Ishikawa,[21,17] R. Itoh,[21,17] M. Iwasaki,[70] Y. Iwasaki,[21] W. W. Jacobs,[30] E.-J. Jang,[18] S. Jia,[13] Y. Jin,[90] K. K. Joo,[6] J. Kahn,[40] A. B. Kaliyar,[85] K. H. Kang,[41] G. Karyan,[9] T. Kawasaki,[42] H. Kichimi,[21] C. Kiesling,[54] C. H. Kim,[19] D. Y. Kim,[81] K.-H. Kim,[96] Y.-K. Kim,[96] P. Kodyš,[5] T. Konno,[42] A. Korobov,[4,69] S. Korpar,[53,39] E. Kovalenko,[4,69] P. Križan,[49,39] R. Kroeger,[56] P. Krokovny,[4,69] T. Kuhr,[50] R. Kumar,[74] K. Kumara,[94] A. Kuzmin,[4,69,47] Y.-J. Kwon,[96] Y.-T. Lai,[41] T. Lam,[93] J. S. Lange,[14] M. Laurenza,[35,77] S. C. Lee,[46] C. H. Li,[48] J. Li,[46] L. K. Li,[8] Y. B. Li,[13] L. Li Gioi,[54] J. Libby,[29] K. Lieret,[50] D. Liventsev,[94,21] A. Martini,[97] M. Masuda,[89,75] T. Matsuda,[57] D. Matvienko,[4,69,47] S. K. Maurya,[27] F. Meier,[10] M. Merola,[34,61] F. Metzner,[40] K. Miyabayashi,[62] R. Mizuk,[47,23] G. B. Mohanty,[85] R. Mussa,[36] M. Nakao,[21,17] Z. Natkaniec,[65] A. Natochii,[20] L. Nayak,[28] M. Niiyama,[45] N. K. Nisar,[3] S. Nishida,[21,17] K. Ogawa,[67] S. Ogawa,[87] H. Ono,[66,67] P. Oskin,[47] P. Pakhlov,[47,58] G. Pakhlova,[23,47] T. Pang,[73] S. Pardi,[34] H. Park,[46] S.-H. Park,[21] S. Patra,[26] S. Paul,[86,54] T. K. Pedlar,[51] R. Pestotnik,[39] L. E. Piilonen,[93] T. Podobnik,[49,39] V. Popov,[23] E. Prencipe,[24] M. T. Prim,[2] M. Röhrken,[9] A. Rostomyan,[9] N. Rout,[29] G. Russo,[61] D. Sahoo,[37] S. Sandilya,[28] A. Sangal,[8] L. Santelj,[49,39] T. Sanuki,[88] V. Savinov,[73] G. Schnell,[1,25] Y. Seino,[67] K. Senyo,[95] M. E. Sevior,[55] M. Shapkin,[33] C. Sharma,[52] J.-G. Shiu,[64] F. Simon,[54] J. B. Singh,[72,*] A. Sokolov,[33] E. Solovieva,[47] S. Stanič,[68] M. Starič,[39] Z. S. Stottler,[93] M. Sumihama,[15] T. Sumiyoshi,[92] M. Takizawa,[79,22,76] U. Tamponi,[36] K. Tanida,[38] F. Tenchini,[9] M. Uchida,[91] K. Uno,[67] S. Uno,[21,17] P. Urquijo,[55] Y. Usov,[4,69] R. Van Tonder,[2] G. Varner,[20] A. Vinokurova,[4,69] E. Waheed,[21] E. Wang,[73] M.-Z. Wang,[64] X. L. Wang,[13] M. Watanabe,[67] S. Watanuki,[96] E. Won,[44] X. Xu,[80] B. D. Yabsley,[83] W. Yan,[78] S. B. Yang,[44] H. Ye,[9] J. H. Yin,[44] C. Z. Yuan,[31] Y. Zhai,[37] Z. P. Zhang,[78] V. Zhilich,[4,69] and V. Zhukova[47]

(Belle Collaboration)

[1]*Department of Physics, University of the Basque Country UPV/EHU, 48080 Bilbao*
[2]*University of Bonn, 53115 Bonn*
[3]*Brookhaven National Laboratory, Upton, New York 11973*
[4]*Budker Institute of Nuclear Physics SB RAS, Novosibirsk 630090*
[5]*Faculty of Mathematics and Physics, Charles University, 121 16 Prague*
[6]*Chonnam National University, Gwangju 61186*
[7]*Chung-Ang University, Seoul 06974*
[8]*University of Cincinnati, Cincinnati, Ohio 45221*
[9]*Deutsches Elektronen–Synchrotron, 22607 Hamburg*
[10]*Duke University, Durham, North Carolina 27708*
[11]*Institute of Theoretical and Applied Research (ITAR), Duy Tan University, Hanoi 100000*
[12]*Department of Physics, Fu Jen Catholic University, Taipei 24205*
[13]*Key Laboratory of Nuclear Physics and Ion-beam Application (MOE) and Institute of Modern Physics, Fudan University, Shanghai 200443*
[14]*Justus-Liebig-Universität Gießen, 35392 Gießen*
[15]*Gifu University, Gifu 501-1193*
[16]*II. Physikalisches Institut, Georg-August-Universität Göttingen, 37073 Göttingen*
[17]*SOKENDAI (The Graduate University for Advanced Studies), Hayama 240-0193*
[18]*Gyeongsang National University, Jinju 52828*
[19]*Department of Physics and Institute of Natural Sciences, Hanyang University, Seoul 04763*
[20]*University of Hawaii, Honolulu, Hawaii 96822*
[21]*High Energy Accelerator Research Organization (KEK), Tsukuba 305-0801*
[22]*J-PARC Branch, KEK Theory Center, High Energy Accelerator Research Organization (KEK), Tsukuba 305-0801*
[23]*National Research University Higher School of Economics, Moscow 101000*

[24]*Forschungszentrum Jülich, 52425 Jülich*
[25]*IKERBASQUE, Basque Foundation for Science, 48013 Bilbao*
[26]*Indian Institute of Science Education and Research Mohali, SAS Nagar, 140306*
[27]*Indian Institute of Technology Guwahati, Assam 781039*
[28]*Indian Institute of Technology Hyderabad, Telangana 502285*
[29]*Indian Institute of Technology Madras, Chennai 600036*
[30]*Indiana University, Bloomington, Indiana 47408*
[31]*Institute of High Energy Physics, Chinese Academy of Sciences, Beijing 100049*
[32]*Institute of High Energy Physics, Vienna 1050*
[33]*Institute for High Energy Physics, Protvino 142281*
[34]*INFN—Sezione di Napoli, I-80126 Napoli*
[35]*INFN—Sezione di Roma Tre, I-00146 Roma*
[36]*INFN—Sezione di Torino, I-10125 Torino*
[37]*Iowa State University, Ames, Iowa 50011*
[38]*Advanced Science Research Center, Japan Atomic Energy Agency, Naka 319-1195*
[39]*J. Stefan Institute, 1000 Ljubljana*
[40]*Institut für Experimentelle Teilchenphysik, Karlsruher Institut für Technologie, 76131 Karlsruhe*
[41]*Kavli Institute for the Physics and Mathematics of the Universe (WPI), University of Tokyo, Kashiwa 277-8583*
[42]*Kitasato University, Sagamihara 252-0373*
[43]*Korea Institute of Science and Technology Information, Daejeon 34141*
[44]*Korea University, Seoul 02841*
[45]*Kyoto Sangyo University, Kyoto 603-8555*
[46]*Kyungpook National University, Daegu 41566*
[47]*P.N. Lebedev Physical Institute of the Russian Academy of Sciences, Moscow 119991*
[48]*Liaoning Normal University, Dalian 116029*
[49]*Faculty of Mathematics and Physics, University of Ljubljana, 1000 Ljubljana*
[50]*Ludwig Maximilians University, 80539 Munich*
[51]*Luther College, Decorah, Iowa 52101*
[52]*Malaviya National Institute of Technology Jaipur, Jaipur 302017*
[53]*Faculty of Chemistry and Chemical Engineering, University of Maribor, 2000 Maribor*
[54]*Max-Planck-Institut für Physik, 80805 München*
[55]*School of Physics, University of Melbourne, Victoria 3010*
[56]*University of Mississippi, University, Mississippi 38677*
[57]*University of Miyazaki, Miyazaki 889-2192*
[58]*Moscow Physical Engineering Institute, Moscow 115409*
[59]*Graduate School of Science, Nagoya University, Nagoya 464-8602*
[60]*Kobayashi-Maskawa Institute, Nagoya University, Nagoya 464-8602*
[61]*Università di Napoli Federico II, I-80126 Napoli*
[62]*Nara Women's University, Nara 630-8506*
[63]*National Central University, Chung-li 32054*
[64]*Department of Physics, National Taiwan University, Taipei 10617*
[65]*H. Niewodniczanski Institute of Nuclear Physics, Krakow 31-342*
[66]*Nippon Dental University, Niigata 951-8580*
[67]*Niigata University, Niigata 950-2181*
[68]*University of Nova Gorica, 5000 Nova Gorica*
[69]*Novosibirsk State University, Novosibirsk 630090*
[70]*Osaka City University, Osaka 558-8585*
[71]*Pacific Northwest National Laboratory, Richland, Washington 99352*
[72]*Panjab University, Chandigarh 160014*
[73]*University of Pittsburgh, Pittsburgh, Pennsylvania 15260*
[74]*Punjab Agricultural University, Ludhiana 141004*
[75]*Research Center for Nuclear Physics, Osaka University, Osaka 567-0047*
[76]*Meson Science Laboratory, Cluster for Pioneering Research, RIKEN, Saitama 351-0198*
[77]*Dipartimento di Matematica e Fisica, Università di Roma Tre, I-00146 Roma*
[78]*Department of Modern Physics and State Key Laboratory of Particle Detection and Electronics, University of Science and Technology of China, Hefei 230026*
[79]*Showa Pharmaceutical University, Tokyo 194-8543*
[80]*Soochow University, Suzhou 215006*
[81]*Soongsil University, Seoul 06978*

[82]Sungkyunkwan University, Suwon 16419
[83]School of Physics, University of Sydney, New South Wales 2006
[84]Department of Physics, Faculty of Science, University of Tabuk, Tabuk 71451
[85]Tata Institute of Fundamental Research, Mumbai 400005
[86]Department of Physics, Technische Universität München, 85748 Garching
[87]Toho University, Funabashi 274-8510
[88]Department of Physics, Tohoku University, Sendai 980-8578
[89]Earthquake Research Institute, University of Tokyo, Tokyo 113-0032
[90]Department of Physics, University of Tokyo, Tokyo 113-0033
[91]Tokyo Institute of Technology, Tokyo 152-8550
[92]Tokyo Metropolitan University, Tokyo 192-0397
[93]Virginia Polytechnic Institute and State University, Blacksburg, Virginia 24061
[94]Wayne State University, Detroit, Michigan 48202
[95]Yamagata University, Yamagata 990-8560
[96]Yonsei University, Seoul 03722
[97]Deutsches Elektronen-Synchrotron, 22607 Hamburg

(Received 6 December 2021; accepted 21 January 2022; published 8 February 2022)

A search for double-heavy tetraquark state candidates $X_{cc\bar{s}\bar{s}}$ decaying to $D_s^+D_s^+$ and $D_s^{*+}D_s^{*+}$ is presented for the first time using the data samples of 102×10^6 $\Upsilon(1S)$ and 158×10^6 $\Upsilon(2S)$ events, and the data samples at $\sqrt{s} = 10.52$, 10.58, and 10.867 GeV corresponding to integrated luminosities of 89.5, 711.0, and 121.4 fb^{-1}, respectively, accumulated with the Belle detector at the KEKB asymmetric energy electron-positron collider. The invariant-mass spectra of the $D_s^+D_s^+$ and $D_s^{*+}D_s^{*+}$ are studied to search for possible resonances. No significant signals are observed, and the 90% confidence level upper limits on the product branching fractions $[\mathcal{B}(\Upsilon(1S, 2S) \to X_{cc\bar{s}\bar{s}} + \text{anything}) \times \mathcal{B}(X_{cc\bar{s}\bar{s}} \to D_s^+D_s^+(D_s^{*+}D_s^{*+}))]$ in $\Upsilon(1S, 2S)$ inclusive decays and the product values of Born cross section and branching fraction $[\sigma(e^+e^- \to X_{cc\bar{s}\bar{s}} + \text{anything}) \times \mathcal{B}(X_{cc\bar{s}\bar{s}} \to D_s^+D_s^+(D_s^{*+}D_s^{*+}))]$ in e^+e^- collisions at $\sqrt{s} = 10.52$, 10.58, and 10.867 GeV under different assumptions of $X_{cc\bar{s}\bar{s}}$ masses and widths are obtained.

DOI: 10.1103/PhysRevD.105.032002

I. INTRODUCTION

The hadron spectrum was successfully categorized based on the quark model as early as the 1960s [1]. For a long time, all known hadrons could be classified as mesons or baryons with components of a quark-antiquark pair ($q\bar{q}$) or three quarks (qqq), respectively. However, quantum chromodynamics (QCD) also allows the existence of more complex structures, such as the tetraquark, pentaquark, or glueball, which possess properties that are forbidden for conventional hadrons. The states that do not fit into the ordinary $q\bar{q}$ or qqq scheme in the quark model are referred to as exotic states.

The experimental discovery of exotic states began in 2003 with the observation of the $X(3872)$ [2]. This new state did not fit any ordinary $c\bar{c}$ quarkonia in the quark model. After that, the $X(3872)$ was observed in multiple decay modes and confirmed by various experiments [3–5]. Many different theoretical interpretations of this state have been proposed, such as meson molecule, tetraquark, and conventional bound state [6–10]. During the past two decades, there has been considerable world-wide activity in exotic state research using various processes, such as e^+e^- annihilation (e.g., at τ-charm facilities and B factories), hadron collisions (e.g., at the Tevatron and the LHC), or photo- and leptoproduction (e.g., at the SPS, HERA, or at Jefferson Lab), and many exotic state candidates were observed [11,12].

In searches for exotic states, a clear feature that helps distinguish exotic from ordinary hadrons would be a nonzero electric charge in a state which contains a heavy quark-antiquark pair of the same flavor. Such a state must contain at least one more quark-antiquark pair, and is thus not a conventional quark-antiquark meson. Furthermore, a state with a pair of two identical heavy flavor quarks (for example, cc), has even more pronounced features as an exotic state. Very recently, the LHCb experiment announced observation of an open-double-charm state T_{cc}^+ in the $D^0D^0\pi^+$ mass spectrum near threshold [13,14]. It contains two charm quarks and two light quarks,

*University of Petroleum and Energy Studies, Dehradun 248007.

Published by the American Physical Society under the terms of the Creative Commons Attribution 4.0 International license. Further distribution of this work must maintain attribution to the author(s) and the published article's title, journal citation, and DOI. Funded by SCOAP³.

TABLE I. Predicted masses and widths for the $X_{cc\bar{s}\bar{s}}$ resonances in $D_s^+D_s^+$ and $D_s^{*+}D_s^{*+}$ final states [19].

Mode	IJ^P	Mass (MeV/c^2)	Width (MeV)
$X_{cc\bar{s}\bar{s}} \to D_s^+D_s^+$	00^+	4902	3.54
$X_{cc\bar{s}\bar{s}} \to D_s^{*+}D_s^{*+}$	02^+	4821	5.58
	02^+	4846	10.68
	02^+	4775	23.26

thus it is a clear evidence for an exotic state. On the theoretical side, in addition to tetraquark models based on a heavy quark pair and two light quarks, the double-heavy tetraquark states are studied using QCD sum rules [15], quark models [16,17], and lattice QCD computations [18]. Besides, a QCD-inspired chiral quark model gives a prediction on the tetraquark states denoted as $X_{cc\bar{s}\bar{s}}$ with $+2$ electric charge in spin-parity channels $J^P = 0^+$ and 2^+, which are expected to be found in $D_s^+D_s^+$ and $D_s^{*+}D_s^{*+}$ final states [19]. The predicted masses and widths of those resonances are listed in Table I. Among the three predicted resonances in $D_s^{*+}D_s^{*+}$ final state, the narrowest one has the highest observable probability.

In this paper, we present a search for double-heavy tetraquark candidates using the $D_s^+D_s^+$ and $D_s^{*+}D_s^{*+}$ final states in $\Upsilon(1S, 2S)$ inclusive decays, and $e^+e^- \to D_s^+D_s^+(D_s^{*+}D_s^{*+}) +$ anything processes at $\sqrt{s} = 10.52$, 10.58, and 10.867 GeV. The D_s^{*+} candidates are reconstructed in decays to $D_s^+\gamma$, while the D_s^+ candidates are reconstructed in the $D_s^+ \to \phi(\to K^+K^-)\pi^+$ and $\bar{K}^*(892)^0(\to K^-\pi^+)K^+$ decays. Inclusion of charged-conjugate modes is implicitly assumed throughout this analysis.

II. THE DATA SAMPLE AND THE BELLE DETECTOR

The data samples used in this analysis include: a 5.74 fb^{-1} data sample collected at the $\Upsilon(1S)$ peak [102×10^6 $\Upsilon(1S)$ events], a 24.7 fb^{-1} data sample collected at the $\Upsilon(2S)$ peak [158×10^6 $\Upsilon(2S)$ events], an 89.5 fb^{-1} data sample collected at $\sqrt{s} = 10.52$ GeV, a 711 fb^{-1} data sample collected at $\sqrt{s} = 10.58$ GeV, and a 121.4 fb^{-1} data sample collected at $\sqrt{s} = 10.867$ GeV, where s is the center-of-mass energy squared. All the data were collected with the Belle detector, which is described in detail in Ref. [20], operating at the KEKB asymmetric-energy e^+e^- collider [21]. It is a large-solid-angle magnetic spectrometer consisting of a silicon vertex detector, a 50-layer central drift chamber, an array of aerogel threshold Cherenkov counters, a barrel-like arrangement of time-of-flight scintillation counters, and an electromagnetic calorimeter comprising CsI(Tl) crystals located inside a superconducting solenoid coil that provides a 1.5 T magnetic field. An iron flux return comprising resistive plate chambers placed outside the coil was instrumented to detect K_L^0 mesons and to identify muons.

Monte Carlo (MC) signal events are generated with EVTGEN [22] and processed through a full simulation of the Belle detector based on GEANT3 [23]. Initial-state radiation (ISR) is taken into account assuming that the cross sections follow a $1/s$ dependence in $e^+e^- \to X_{cc\bar{s}\bar{s}} +$ anything reactions. The processes $\Upsilon(1S, 2S) \to D_s^+D_s^+(D_s^{*+}D_s^{*+}) +$ anything and $e^+e^- \to D_s^+D_s^+(D_s^{*+}D_s^{*+}) +$ anything at $\sqrt{s} = 10.52$, 10.58, and 10.867 GeV are taken into account, where the D_s^{*+} decays into $D_s^+\gamma$ using a P-wave model, and the D_s^+ decays to $K^+K^-\pi^+$ final states using a Dalitz plot decay model of Ref. [24]. The mass of $X_{cc\bar{s}\bar{s}}$ is chosen in the interval from 4882 to 4922 MeV/c^2 (4801 to 4841 MeV/c^2) in steps of 5 MeV/c^2, with a width varying from 0.54 to 6.54 MeV (2.58 to 8.58 MeV) in steps of 1 MeV for $X_{cc\bar{s}\bar{s}} \to D_s^+D_s^+$ ($D_s^{*+}D_s^{*+}$). Inclusive MC samples of $\Upsilon(1S, 2S)$ decays, $\Upsilon(4S) \to B^+B^-/B^0\bar{B}^0$, $\Upsilon(5S) \to B_s^{(*)}\bar{B}_s^{(*)}$, and $e^+e^- \to q\bar{q}$ ($q = u$, d, s, c) at $\sqrt{s} = 10.52$, 10.58, and 10.867 GeV corresponding to four times the integrated luminosity of data are used to study possible peaking backgrounds.

III. COMMON EVENT SELECTION CRITERIA

For reconstructed charged tracks, the impact parameters perpendicular to and along the beam direction with respect to the interaction point are required to be less than 0.2 cm and 1.5 cm, respectively, and the transverse momentum in the laboratory frame is required to be larger than 0.1 GeV/c. For the particle identification (PID) of a well-reconstructed charged track, information from different detector subsystems, including specific ionization in the central drift chamber, time measurement in the time-of-flight scintillation counters, and the response of the aerogel threshold Cherenkov counters, is combined to form a likelihood $\mathcal{L}_i$ [25] for particle species i, where $i = \pi$ or K. Tracks with $R_K = \mathcal{L}_K/(\mathcal{L}_K + \mathcal{L}_\pi) < 0.4$ are identified as pions with an efficiency of 96%, while 5% of kaons are misidentified as pions; tracks with $R_K > 0.6$ are identified as kaons with an efficiency of 95%, while 4% of pions are misidentified as kaons.

An electromagnetic calorimeter cluster is taken as a photon candidate if it does not match the extrapolation of any charged tracks. The energy of the photon candidate from the D_s^{*+} decay is required to be greater than 50 MeV. For D_s^+ candidates, vertex and mass-constrained fits are performed, and then $\chi^2_{\mathrm{vertex}}/\mathrm{n.d.f} < 20$ is required (>97% selection efficiency according to MC simulation). For D_s^{*+} candidates, a mass-constrained fit is performed to improve its momentum resolution. The best D_s^{*+} candidate with χ^2 of D_s^{*+} mass-constrained fit for each D_s^+ candidate is kept to suppress the combinational background.

The signal mass windows for $\bar{K}^*(892)^0$, ϕ, D_s^+, and D_s^{*+} candidates have been optimized by maximizing the Punzi

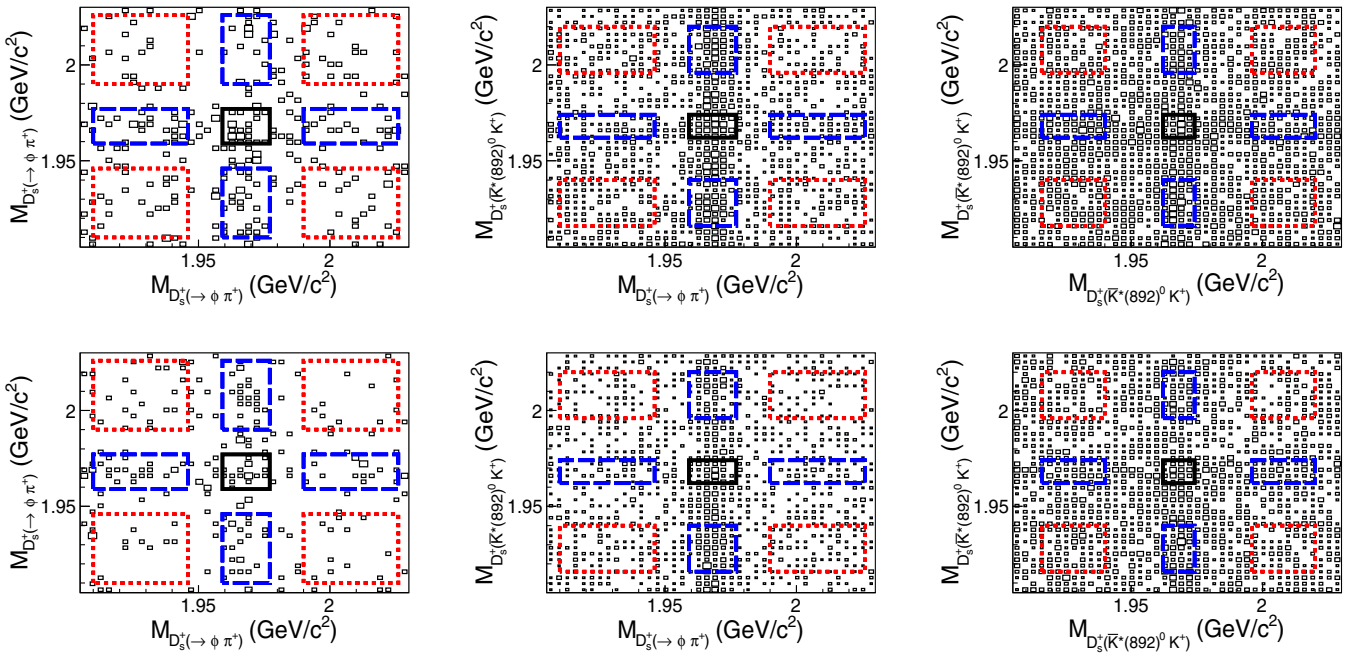

FIG. 1. The top (bottom) plots show the distribution of $M_{D_s^+}$ vs $M_{D_s^+}$ from the selected $e^+e^- \to X_{cc\bar{s}\bar{s}} \to D_s^+ D_s^+ (D_s^{*+} D_s^{*+}) +$ anything candidates from data at $\sqrt{s} = 10.58$ GeV, where the D_s^+ is reconstructed from $\phi\pi^+$ or $\bar{K}^*(892)^0 K^+$. The central solid boxes define the signal regions, and the red dash-dotted and blue dashed boxes show the $M_{D_s^+}$ sideband regions described in the text.

parameter $S/(3/2 + \sqrt{B})$ [26], where S is the number of selected events in the simulated signal process by fitting the $X_{cc\bar{s}\bar{s}}$ invariant-mass spectrum. B is the number of selected events obtained from the normalized $M_{D_s^+ D_s^+}$ sidebands in inclusive MC samples. The optimized mass window requirements are $|M_{K^+K^-} - m_\phi| < 8$ MeV/c^2, $|M_{\phi\pi^+} - m_{D_s^+}| < 7$ MeV/c^2, $|M_{K^-\pi^+} - m_{\bar{K}^*(892)^0}| < 50$ MeV/c^2, $|M_{\bar{K}^*(892)^0 K^+} - m_{D_s^+}| < 7$ MeV/c^2, and $|M_{\gamma D_s^+} - m_{D_s^{*+}}| < 14$ MeV/c^2, where m_ϕ, $m_{\bar{K}^*(892)^0}$, $m_{D_s^+}$, and $m_{D_s^{*+}}$ are the nominal masses of ϕ, $\bar{K}^*(892)^0$, D_s^+, and D_s^{*+} [27]. There are no multiple candidates after processing all selections in both $D_s^+ D_s^+$ and $D_s^{*+} D_s^{*+}$ cases. Figure 1 shows the scatter plots of D_s^+ versus D_s^+ invariant masses from the selected $e^+e^- \to X_{cc\bar{s}\bar{s}} (\to D_s^+ D_s^+ (D_s^{*+} D_s^{*+})) +$ anything candidates from data at $\sqrt{s} = 10.58$ GeV as an example. Here we define the two-dimensional $D_s^+ D_s^+$ sidebands, and the normalized contribution from D_s^+ and D_s^+ sidebands is estimated using 25% of the number of events in the blue dashed line boxes and reduced by 6.25% of the number of events in the red dotted line boxes.

IV. INVARIANT-MASS SPECTRA

The $D_s^+ D_s^+$ and $D_s^{*+} D_s^{*+}$ invariant mass distributions of selected events from data samples in the kinematically allowed region are shown in Figs. 2 and 3 together with the backgrounds estimated from the normalized $D_s^+ D_s^+$ sideband events. No peaking backgrounds are found in the normalized sideband events in either $D_s^+ D_s^+$ and $D_s^{*+} D_s^{*+}$ invariant mass distributions from data, nor in the $D_s^+ D_s^+$ and $D_s^{*+} D_s^{*+}$ mass spectra from inclusive MC samples [28]. Thus in the following we only focus on the mass spectra from the theoretically predicted regions for $X_{cc\bar{s}\bar{s}}$ [19] which are shown in Figs. 4 and 5.

Since no clear signals are observed in the invariant-mass spectra, the 90% confidence level (CL) upper limits on the numbers of signal events are given. The upper limit is calculated by the frequentist approach [29] implemented in the Poissonian limit estimator program [30], where the mass window is obtained by giving 95% acceptance to the corresponding simulated signal events, the number of signal candidate events is counted directly, and the number of expected background events is estimated from the normalized mass sidebands. The possible nonresonant contributions in the $D_s^+ D_s^+$ and $D_s^{*+} D_s^{*+}$ invariant-mass spectra are not subtracted and taken as potential signals, in order to set more conservative upper limits.

The upper limit calculation is repeated with $M_{X_{cc\bar{s}\bar{s}}}$ varying from 4882 to 4922 MeV/c^2 in steps of 5 MeV/c^2 and $\Gamma_{X_{cc\bar{s}\bar{s}}}$ varying from 0.54 to 6.54 MeV in steps of 1.0 MeV for the $M_{D_s^+ D_s^+}$ distribution, and with $M_{X_{cc\bar{s}\bar{s}}}$ varying from 4801 to 4841 MeV/c^2 in steps of 5 MeV/c^2 and $\Gamma_{X_{cc\bar{s}\bar{s}}}$ varying from 2.58 to 8.58 MeV in steps of 1.0 MeV for the $M_{D_s^{*+} D_s^{*+}}$ distribution.

V. SYSTEMATIC UNCERTAINTIES

There are several sources of systematic uncertainties on the branching fraction and Born cross section

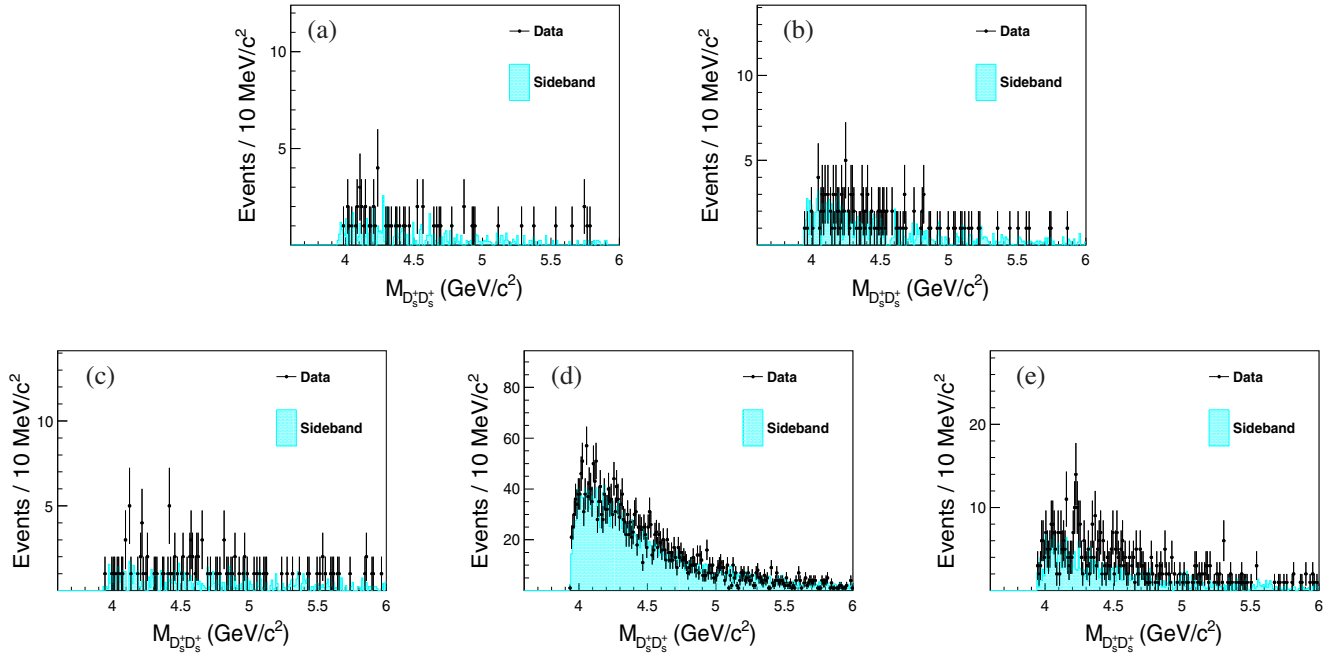

FIG. 2. Distributions of $M_{D_s^+D_s^+}$ from data for processes (a) $\Upsilon(1S) \to X_{cc\bar{s}\bar{s}}(\to D_s^+ D_s^+) + \text{anything}$, (b) $\Upsilon(2S) \to X_{cc\bar{s}\bar{s}}(\to D_s^+ D_s^+) + \text{anything}$, and $e^+e^- \to X_{cc\bar{s}\bar{s}}(\to D_s^+ D_s^+) + \text{anything}$ at (c) $\sqrt{s} = 10.52$ GeV, (d) $\sqrt{s} = 10.58$ GeV, (e) $\sqrt{s} = 10.867$ GeV. The cyan shaded histograms are from the normalized $M_{D_s^+D_s^+}$ sideband events.

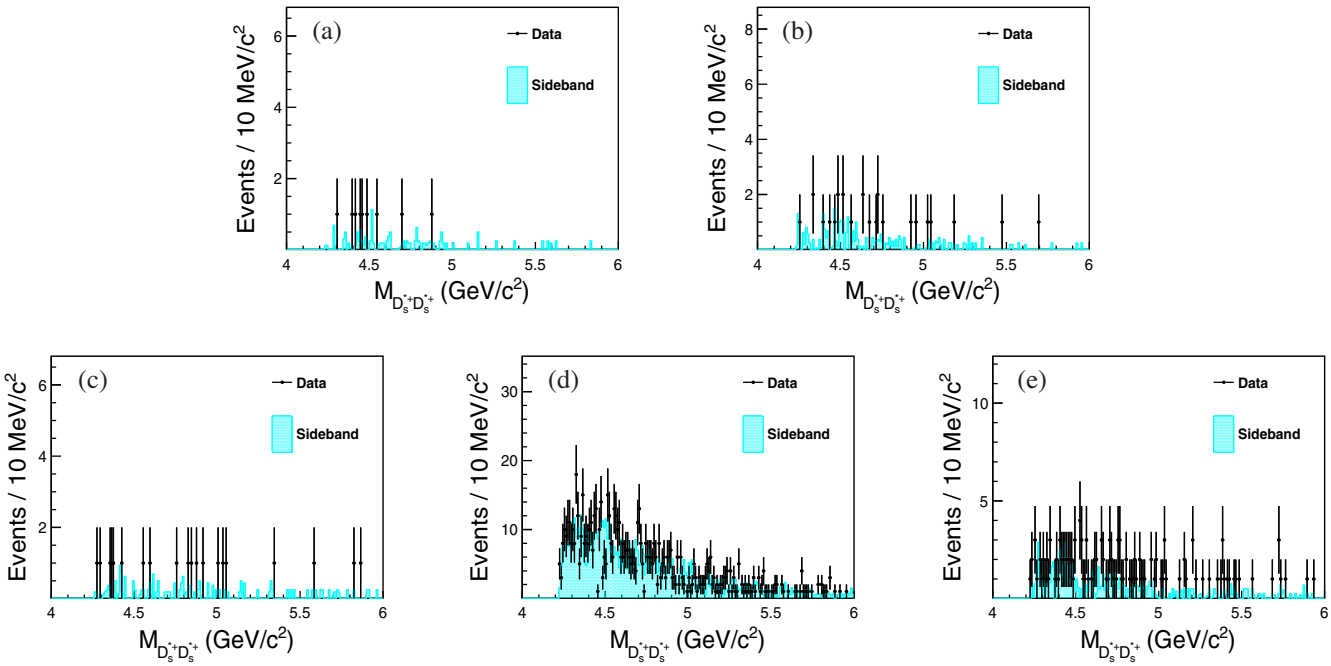

FIG. 3. Distributions of $M_{D_s^{*+}D_s^{*+}}$ from data for processes (a) $\Upsilon(1S) \to X_{cc\bar{s}\bar{s}}(\to D_s^{*+} D_s^{*+}) + \text{anything}$, (b) $\Upsilon(2S) \to X_{cc\bar{s}\bar{s}}(\to D_s^{*+} D_s^{*+}) + \text{anything}$, and $e^+e^- \to X_{cc\bar{s}\bar{s}}(\to D_s^{*+} D_s^{*+}) + \text{anything}$ at (c) $\sqrt{s} = 10.52$ GeV, (d) $\sqrt{s} = 10.58$ GeV, (e) $\sqrt{s} = 10.867$ GeV. The cyan shaded histograms are from the normalized $M_{D_s^+D_s^+}$ sideband events.

measurements, which can be divided into multiplicative and additive systematic uncertainties. The multiplicative systematic uncertainties include detection-efficiency-related (DER) sources (tracking efficiency, PID, and photon reconstruction), the statistical uncertainty of the MC efficiency, branching fractions of intermediate states, the total numbers of $\Upsilon(1S)$ and $\Upsilon(2S)$ events, and the integrated luminosities at $\sqrt{s} = 10.52$, 10.58, and 10.867 GeV.

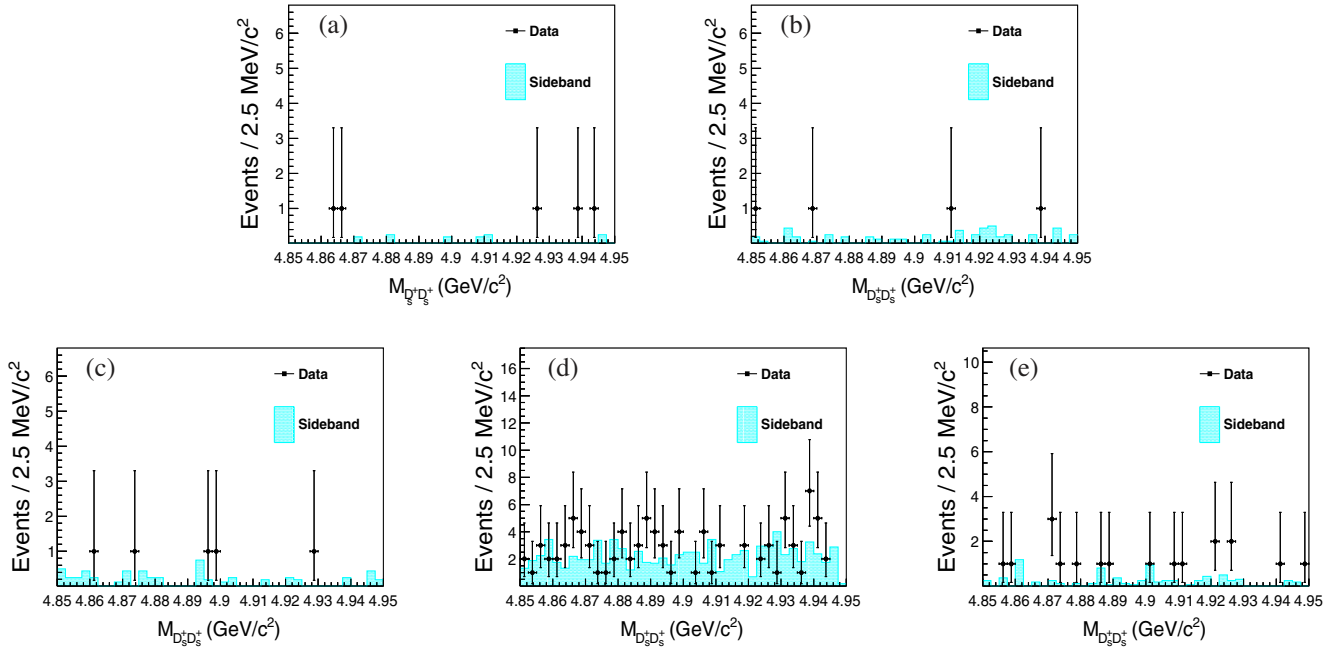

FIG. 4. Distributions of $M_{D_s^+D_s^+}$ from data for processes (a) $\Upsilon(1S) \to X_{cc\bar{s}\bar{s}}(\to D_s^+ D_s^+) + \text{anything}$, (b) $\Upsilon(2S) \to X_{cc\bar{s}\bar{s}}(\to D_s^+ D_s^+) + \text{anything}$, and $e^+e^- \to X_{cc\bar{s}\bar{s}}(\to D_s^+ D_s^+) + \text{anything}$ at (c) $\sqrt{s} = 10.52$ GeV, (d) $\sqrt{s} = 10.58$ GeV, (e) $\sqrt{s} = 10.867$ GeV. The cyan shaded histograms are from the normalized $M_{D_s^+D_s^+}$ sideband events.

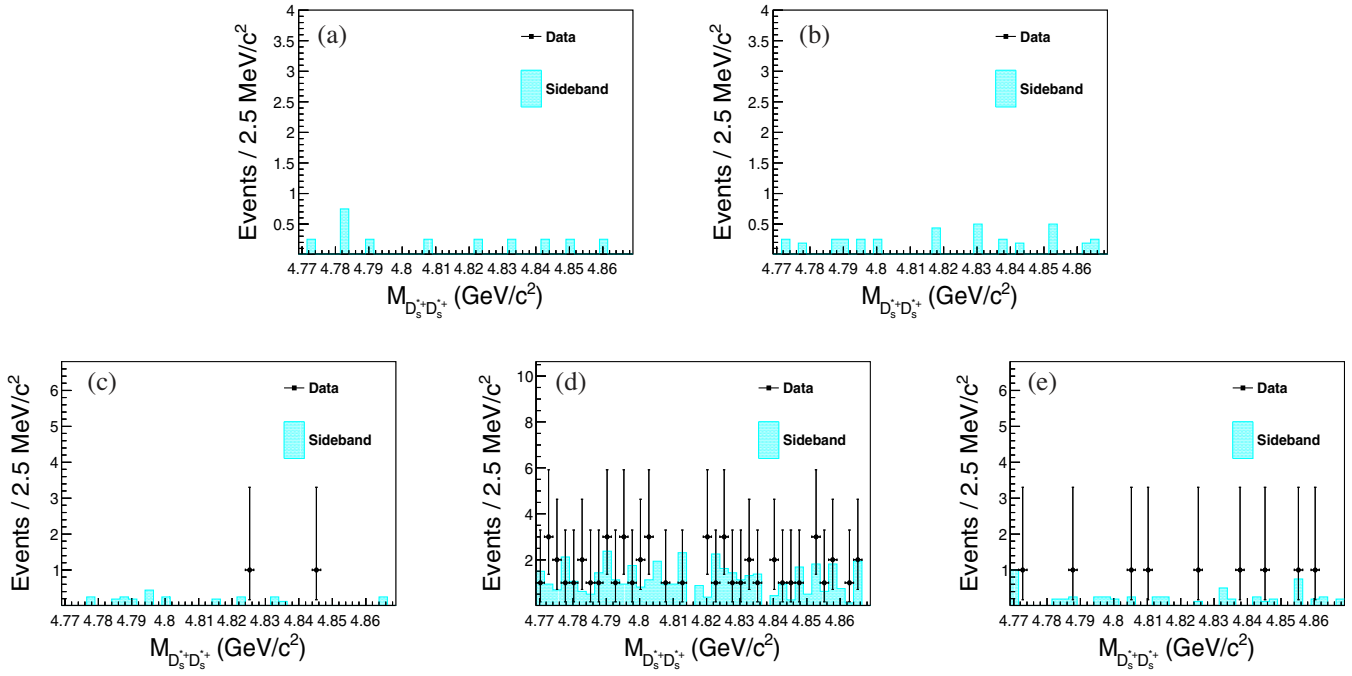

FIG. 5. Distributions of $M_{D_s^{*+}D_s^{*+}}$ from data for processes (a) $\Upsilon(1S) \to X_{cc\bar{s}\bar{s}}(\to D_s^{*+} D_s^{*+}) + \text{anything}$, (b) $\Upsilon(2S) \to X_{cc\bar{s}\bar{s}}(\to D_s^{*+} D_s^{*+}) + \text{anything}$, and $e^+e^- \to X_{cc\bar{s}\bar{s}}(\to D_s^{*+} D_s^{*+}) + \text{anything}$ at (c) $\sqrt{s} = 10.52$ GeV, (d) $\sqrt{s} = 10.58$ GeV, (e) $\sqrt{s} = 10.867$ GeV. The cyan shaded histograms are from the normalized $M_{D_s^+D_s^+}$ sideband events.

The systematic uncertainties related to detection efficiency (σ_{DER}) include the tracking efficiency (0.35% per track, estimated using partially reconstructed D^* decays in $D^{*+} \to \pi^+ D^0, D^0 \to K_S^0 \pi^+ \pi^-$), PID efficiency (2.2% per kaon and 1.8% per pion, estimated using $D^{*+} \to D^0 \pi^+$, $D^0 \to K^- \pi^+$ samples), and photon reconstruction (2.0% per photon, estimated using a radiative Bhabha sample). The statistical uncertainty in the signal MC simulation

TABLE II. Summary of the multiplicative systematic uncertainties (%) on the branching fraction measurements for $\Upsilon(1S,2S) \to X_{cc\bar{s}\bar{s}}(\to D_s^+ D_s^+ (D_s^{*+} D_s^{*+})) +$ anything and on the Born cross section measurements for $e^+e^- \to X_{cc\bar{s}\bar{s}}(\to D_s^+ D_s^+ (D_s^{*+} D_s^{*+})) +$ anything at $\sqrt{s} = 10.52$, 10.58, and 10.867 GeV.

$M_{D_s^+ D_s^+}$ ($M_{D_s^{*+} D_s^{*+}}$) mode	DER	MC statistic	ISR	$\mathcal{B}$	$[N_{\Upsilon(1S)}/N_{\Upsilon(2S)}/\mathcal{L}]$	Sum
$\Upsilon(1S) \to X_{cc\bar{s}\bar{s}} +$ anything	6.1 (7.3)	1.0	—	3.0	2.0	7.2 (8.2)
$\Upsilon(2S) \to X_{cc\bar{s}\bar{s}} +$ anything	6.1 (7.3)	1.0	—	3.0	2.3	7.2 (8.3)
$e^+e^- \to X_{cc\bar{s}\bar{s}} +$ anything at $\sqrt{s} = 10.52$ GeV	6.1 (7.3)	1.0	0.3	3.0	1.4	7.0 (8.2)
$e^+e^- \to X_{cc\bar{s}\bar{s}} +$ anything at $\sqrt{s} = 10.58$ GeV	6.1 (7.3)	1.0	0.3	3.0	1.4	7.0 (8.2)
$e^+e^- \to X_{cc\bar{s}\bar{s}} +$ anything at $\sqrt{s} = 10.867$ GeV	6.1 (7.3)	1.0	0.3	3.0	1.4	7.0 (8.2)

efficiency can be calculated as $\Delta\varepsilon = \sqrt{\varepsilon(1-\varepsilon)/N}$, where ε is the reconstruction efficiency after all event selections, and N is the total number of generated events. Its relative uncertainty $\sigma_{\text{MC stat}} = \Delta\varepsilon/\varepsilon$ is at most at the 1.0% level. Changing the s dependence of the cross sections of $e^+e^- \to X_{cc\bar{s}\bar{s}}(\to D_s^{*+} D_s^{*+}) +$ anything from $1/s$ to $1/s^4$, the product of efficiency and radiative correction factor $\epsilon(1+\delta)_{\text{ISR}}$ changes by less than 0.3% (σ_{ISR}).

The relative uncertainties of branching fractions for $D_s^{*+} \to \gamma D_s^+$, $D_s^+ \to \phi(\to K^+K^-)\pi^+$, and $D_s^+ \to \bar{K}^*(892)^0(\to K^-\pi^+)K^+$ are 0.75%, 3.52%, and 3.45% [27], respectively. The total uncertainties are calculated using $\sigma_{\mathcal{B}} = \frac{\sqrt{\Sigma(\varepsilon_i \times \mathcal{B}_i \times \sigma_{\mathcal{B}_i})^2}}{\Sigma(\varepsilon_i \times \mathcal{B}_i)}$, where ε_i is the efficiency, $\sigma_{\mathcal{B}_i}$ is the relative uncertainty of intermediate states' branching fractions, and $\mathcal{B}_i$ is the product of branching fractions of the intermediate states for each reconstructed mode i.

The total numbers of $\Upsilon(1S)$ and $\Upsilon(2S)$ events are estimated to be $(102 \pm 2) \times 10^6$ and $(157.8 \pm 3.6) \times 10^6$, which are determined by counting the numbers of inclusive hadrons. The uncertainties are mainly due to imperfect simulations of the charged multiplicity distributions from inclusive hadronic MC events ($\sigma_{N_{\Upsilon(1S,2S)}}$). Belle measures luminosity with 1.4% precision using wide angle Bhabha events ($\sigma_{\mathcal{L}}$).

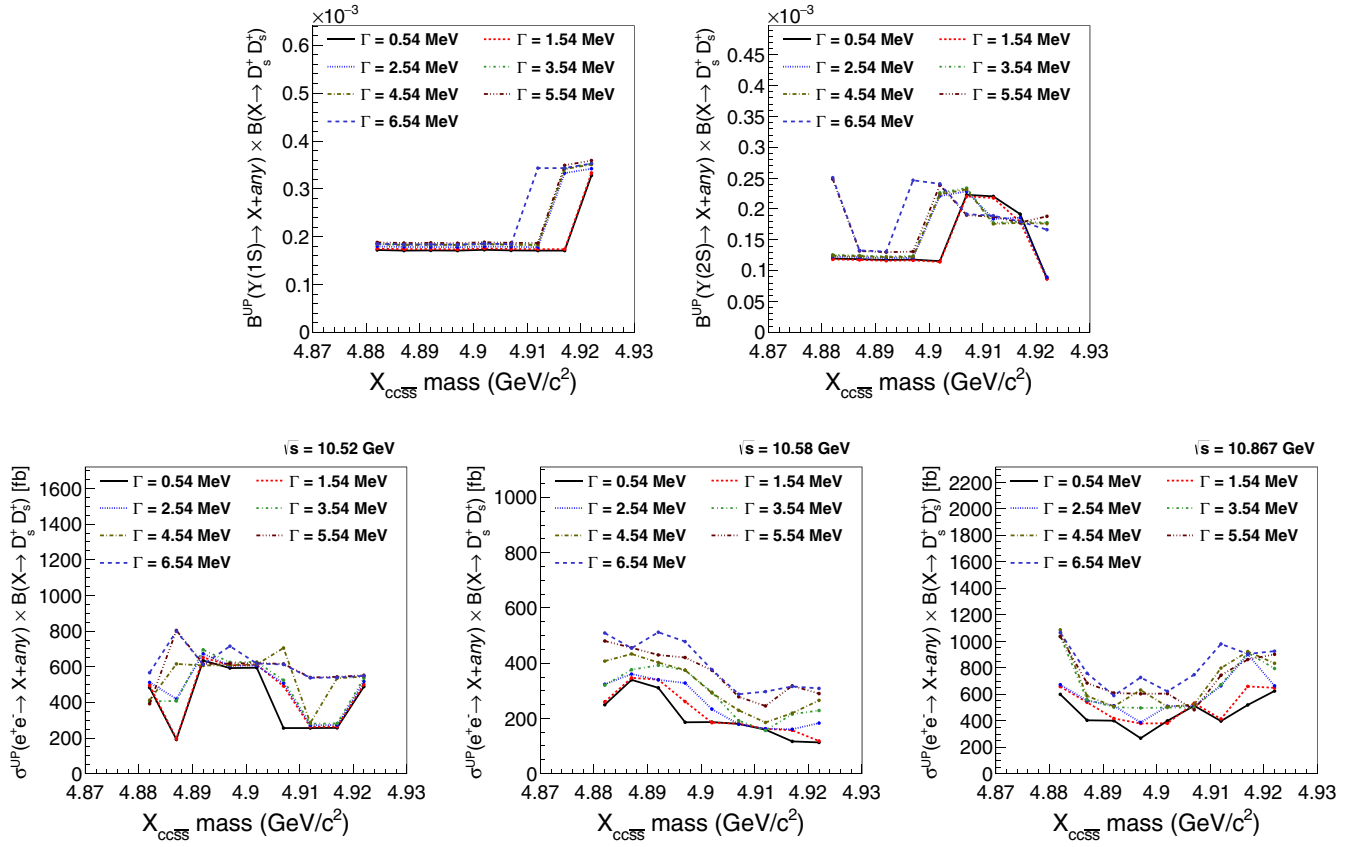

FIG. 6. The 90% CL upper limits on the product branching fractions of $\Upsilon(1S,2S) \to X_{cc\bar{s}\bar{s}}(\to D_s^+ D_s^+) +$ anything and the Born cross sections of $e^+e^- \to X_{cc\bar{s}\bar{s}} +$ anything at $\sqrt{s} = 10.52$, 10.58, and 10.867 GeV with $M_{X_{cc\bar{s}\bar{s}}}$ varying from 4882 to 4922 MeV/c^2 in steps of 5 MeV/c^2 and $\Gamma_{X_{cc\bar{s}\bar{s}}}$ varying from 0.54 to 6.54 MeV in steps of 1.0 MeV.

All the multiplicative uncertainties are summarized in Table II for the measurements of $\Upsilon(1S,2S) \to X_{cc\bar{s}\bar{s}} +$ anything and $e^+e^- \to X_{cc\bar{s}\bar{s}} +$ anything at $\sqrt{s} = 10.52$, 10.58, and 10.867 GeV, respectively. The total multiplicative uncertainty is calculated by adding all sources of multiplicative uncertainty in quadrature,

$$\sigma_{\rm syst} = \sqrt{\sigma^2_{\rm DER} + \sigma^2_{\rm MC\,stat} + \sigma^2_{\rm ISR} + \sigma^2_{\mathcal{B}} + \sigma^2_{\rm N_{\Upsilon(1S,2S)/\mathcal{L}}}}.$$

The additive uncertainty due to the number of expected background is considered by counting normalized background distributions directly, fitting the distributions with a constant, and a first-order polynominal.

VI. STATISTICAL INTERPRETATION OF UPPER LIMIT SETTING

Since no signal traces are observed in the $D_s^+D_s^+$ or $D_s^{*+}D_s^{*+}$ distributions from data at all energy points, the 90% CL upper limits on the numbers of signal events ($N^{\rm UP}$) are determined. To take into account the additive and multiplicative uncertainties, we first study the additive systematic uncertainty and take the most conservative case, then use the total multiplicative systematic uncertainty as an input parameter to the Poissonian limit estimator program.

Since there are few events observed from data sample at $\sqrt{s} = 10.52$ GeV, the continuum contributions are neglected for the $\Upsilon(1S,2S)$ decays. The conservative upper limit on the product branching fractions in $\Upsilon(1S,2S)$ decays $\mathcal{B}^{\rm UP}(\Upsilon(1S,2S) \to X_{cc\bar{s}\bar{s}} + \text{anything}) \times \mathcal{B}(X_{cc\bar{s}\bar{s}} \to D_s^+D_s^+(D_s^{*+}D_s^{*+}))$ are obtained by the following formula:

$$\frac{N^{\rm UP}}{N_{\Upsilon(1S,2S)} \times \sum_i \varepsilon_i \mathcal{B}_i},$$

where $N^{\rm UP}$ is the 90% CL upper limit on the number of events from the data signal yields including all systematic uncertainties that are mentioned above from other variables in this expression, $N_{\Upsilon(1S,2S)}$ is the total number of $\Upsilon(1S,2S)$ events, ε_i is the corresponding detection efficiency, and $\mathcal{B}_i$ is the product of all secondary branching fractions for each reconstructed channel.

The conservative upper limit on the product values of Born cross section and branching fraction $\sigma^{\rm UP}(e^+e^- \to X_{cc\bar{s}\bar{s}} + \text{anything}) \times \mathcal{B}(X_{cc\bar{s}\bar{s}} \to D_s^+D_s^+(D_s^{*+}D_s^{*+}))$ are calculated by the following formula:

$$\frac{N^{\rm UP} \times |1-\Pi|^2}{\mathcal{L} \times \sum_i \varepsilon_i \mathcal{B}_i \times (1+\delta)_{\rm ISR}},$$

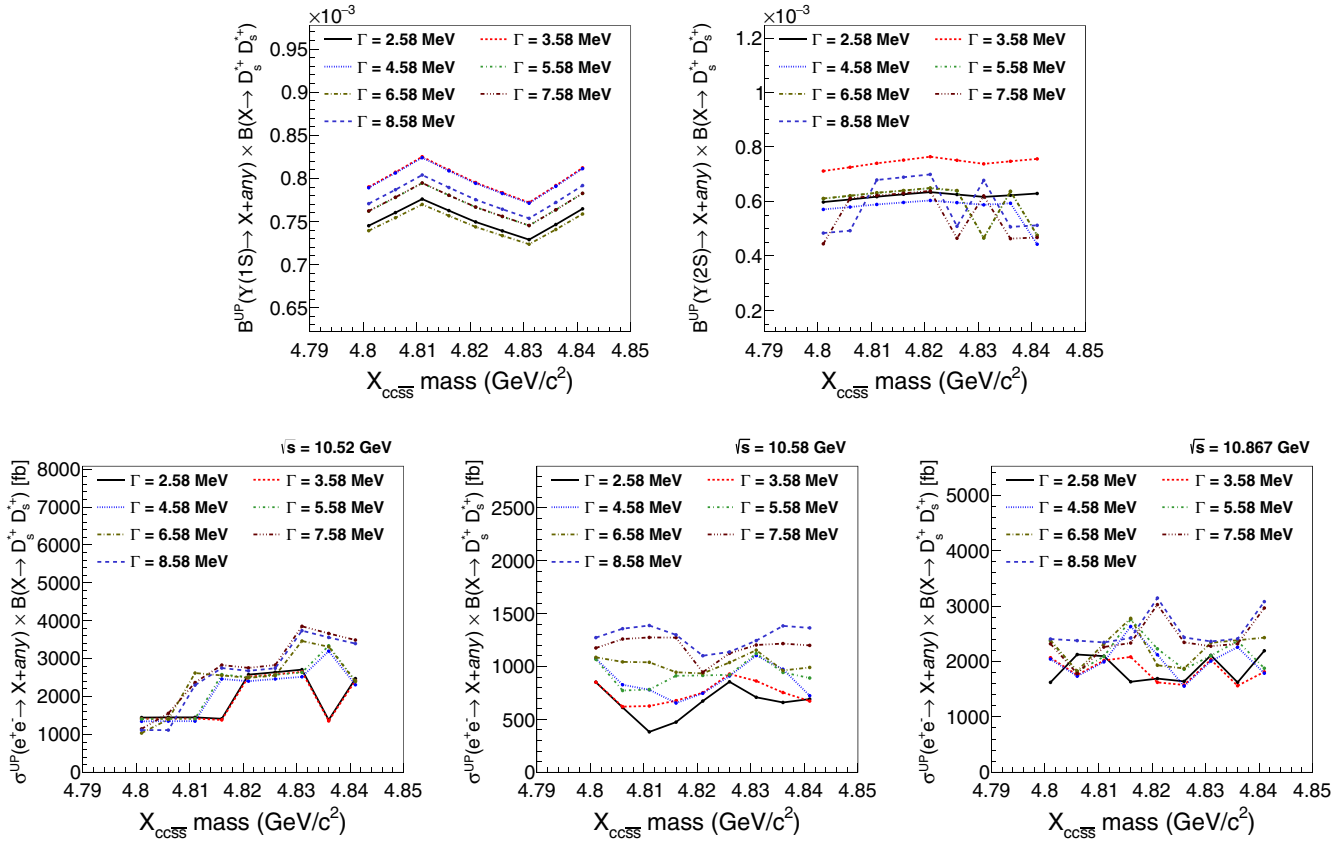

FIG. 7. The 90% CL upper limits on the product branching fractions of $\Upsilon(1S,2S) \to X_{cc\bar{s}\bar{s}}(\to D_s^{*+}D_s^{*+}) +$ anything and the Born cross sections of $e^+e^- \to X_{cc\bar{s}\bar{s}} +$ anything at $\sqrt{s} = 10.52$, 10.58, and 10.867 GeV with $M_{X_{cc\bar{s}\bar{s}}}$ varying from 4801 to 4841 MeV/c^2 in steps of 5 MeV/c^2 and $\Gamma_{X_{cc\bar{s}\bar{s}}}$ varying from 2.58 to 8.58 MeV in steps of 1.0 MeV.

where N^{UP} is the 90% CL upper limit on the number of events in data signal yields including all systematic uncertainties that are mentioned above from other variables in this expression, $|1-\Pi|^2$ is the vacuum polarization factor, $\mathcal{L}$ is the integrated luminosity, ε_i is the corresponding detection efficiency, $\mathcal{B}_{\mathrm{i}}$ is the product of all secondary branching fractions for each reconstructed channel, and $(1+\delta)_{\mathrm{ISR}}$ is the radiative correction factor. The values of

TABLE III. Summary of 90% CL upper limits with the systematic uncertainties included on the product branching fractions of $\Upsilon(1S)/\Upsilon(2S) \to X_{cc\bar{s}\bar{s}}(\to D_s^+ D_s^+) + \text{anything}$.

$\mathcal{B}(\Upsilon(1S)/\Upsilon(2S) \to X_{cc\bar{s}\bar{s}} + \text{anything}) \times \mathcal{B}(X_{cc\bar{s}\bar{s}} \to D_s^+ D_s^+)$ $(\times 10^{-4})$							
	$\Gamma_{X_{cc\bar{s}\bar{s}}}$ (MeV)						
$M_{X_{cc\bar{s}\bar{s}}}$ (MeV/c^2)	0.54	1.54	2.54	3.54	4.54	5.54	6.54
4882	1.7/1.2	1.7/1.2	1.8/1.2	1.8/1.3	1.8/1.2	1.9/2.5	1.9/2.5
4887	1.7/1.2	1.7/1.2	1.8/1.2	1.8/1.2	1.8/1.2	1.9/1.3	1.8/1.3
4892	1.7/1.2	1.7/1.2	1.8/1.2	1.8/1.2	1.8/1.2	1.9/1.3	1.8/1.3
4897	1.7/1.2	1.7/1.2	1.8/1.2	1.8/1.2	1.8/1.2	1.9/1.3	1.8/2.5
4902	1.7/1.2	1.8/1.1	1.8/2.2	1.8/2.3	1.8/2.2	1.9/2.4	1.9/2.4
4907	1.7/2.2	1.7/2.2	1.8/2.3	1.8/2.3	1.8/2.3	1.9/1.9	1.8/1.9
4912	1.7/2.2	1.7/2.2	1.8/1.8	1.8/1.8	1.8/1.8	1.9/1.9	3.4/1.9
4917	1.7/1.9	1.7/1.8	3.3/1.9	3.4/1.8	3.4/1.8	3.5/1.8	3.4/1.8
4922	3.3/0.9	3.3/0.9	3.4/0.9	3.5/1.8	3.5/1.8	3.6/1.9	3.5/1.7

TABLE IV. Summary of 90% CL upper limits with the systematic uncertainties included on the cross sections of $e^+e^- \to X_{cc\bar{s}\bar{s}}(\to D_s^+ D_s^+) + \text{anything}$ at $\sqrt{s} = 10.52/10.58/10.867$ GeV.

$\sigma(e^+e^- \to X_{cc\bar{s}\bar{s}} + \text{anything}) \times \mathcal{B}(X_{cc\bar{s}\bar{s}} \to D_s^+ D_s^+)$ $(\times 10^2 fb)$							
	$\Gamma_{X_{cc\bar{s}\bar{s}}}$ (MeV)						
$M_{X_{cc\bar{s}\bar{s}}}$ (MeV/c^2)	0.54	1.54	2.54	3.54	4.54	5.54	6.54
4882	4.8/2.5/6.0	5.0/2.6/6.6	5.1/3.2/6.7	4.1/3.2/10.3	4.1/4.1/10.9	3.9/4.8/10.4	5.7/5.1/10.6
4887	1.9/3.4/4.0	2.0/3.5/5.4	4.2/3.6/5.5	4.1/3.8/5.6	6.2/4.3/5.9	8.0/4.6/6.8	8.0/4.5/7.6
4892	6.4/3.1/4.0	6.5/3.4/4.2	6.7/3.4/5.1	7.0/3.9/5.0	6.1/4.0/5.1	6.2/4.3/6.1	6.1/5.1/5.9
4897	5.9/1.9/2.7	6.1/2.6/3.8	6.0/3.3/3.9	6.2/3.7/5.0	6.1/3.7/6.3	6.2/4.2/6.0	7.2/4.8/7.3
4902	6.0/1.9/4.0	6.1/1.8/3.8	6.1/2.3/5.1	6.3/2.9/5.0	6.1/2.9/5.1	6.2/3.7/6.1	6.2/3.8/6.2
4907	2.6/1.8/5.1	4.9/1.8/5.3	5.1/1.8/5.1	5.2/1.9/5.0	7.1/2.3/5.1	6.2/2.8/4.7	6.1/2.9/7.5
4912	2.6/1.6/4.0	2.6/1.6/4.1	2.7/1.6/6.6	2.8/1.6/6.7	2.9/1.9/7.8	5.4/2.5/7.3	5.4/3.0/9.6
4917	2.6/1.2/5.2	2.6/1.6/6.6	2.7/1.6/9.0	2.8/2.2/9.1	5.4/2.2/9.0	5.4/3.2/8.6	5.4/3.2/8.9
4922	4.9/1.1/6.2	5.0/1.2/6.5	5.2/1.8/6.6	5.4/2.3/7.9	5.4/2.7/8.3	5.5/2.9/9.0	5.5/3.1/9.2

TABLE V. Summary of 90% CL upper limits with the systematic uncertainties included on the product branching fractions of $\Upsilon(1S) \to X_{cc\bar{s}\bar{s}}(\to D_s^{*+} D_s^{*+}) + \text{anything}/\Upsilon(2S) \to X_{cc\bar{s}\bar{s}}(\to D_s^{*+} D_s^{*+}) + \text{anything}$.

$\mathcal{B}(\Upsilon(1S)/\Upsilon(2S) \to X_{cc\bar{s}\bar{s}} + \text{anything}) \times \mathcal{B}(X_{cc\bar{s}\bar{s}} \to D_s^{*+} D_s^{*+})$ $(\times 10^{-4})$							
	$\Gamma_{X_{cc\bar{s}\bar{s}}}$ (MeV)						
$M_{X_{cc\bar{s}\bar{s}}}$ (MeV/c^2)	2.58	3.58	4.58	5.58	6.58	7.58	8.58
4801	7.5/6.0	7.9/7.1	7.9/5.7	7.6/6.1	7.4/6.1	7.6/4.4	7.7/4.8
4806	7.6/6.1	8.1/7.3	8.1/5.8	7.8/6.2	7.5/6.2	7.8/6.1	7.9/4.9
4811	7.8/6.2	8.3/7.4	8.2/5.9	7.9/6.3	7.7/6.3	7.9/6.2	8.0/6.8
4816	7.6/6.3	8.1/7.5	8.1/6.0	7.8/6.4	7.6/6.4	7.8/6.3	7.9/6.9
4821	7.5/6.3	8.0/7.6	7.9/6.0	7.7/6.5	7.4/6.5	7.7/6.4	7.8/7.0
4826	7.4/6.3	7.8/7.5	7.8/6.0	7.6/6.4	7.3/6.4	7.6/4.7	7.6/5.1
4831	7.3/6.2	7.7/7.4	7.7/5.9	7.5/4.7	7.2/4.7	7.5/6.2	7.5/6.8
4836	7.5/6.2	7.9/7.5	7.9/5.9	7.6/6.4	7.4/6.4	7.6/4.6	7.7/5.1
4841	7.6/6.3	8.1/7.6	8.1/4.4	7.8/4.8	7.6/4.8	7.8/4.7	7.9/5.1

TABLE VI. Summary of 90% CL upper limits with the systematic uncertainties included on the cross sections of $e^+e^- \to X_{cc\bar{s}\bar{s}}(\to D_s^{*+}D_s^{*+}) + \text{anything}$ at $\sqrt{s} = 10.52/10.58/10.867$ GeV.

$\sigma(e^+e^- \to X_{cc\bar{s}\bar{s}} + \text{anything}) \times \mathcal{B}(X_{cc\bar{s}\bar{s}} \to D_s^{*+}D_s^{*+})$ $(\times 10^2 fb)$							
$M_{X_{cc\bar{s}\bar{s}}}$	$\Gamma_{X_{cc\bar{s}\bar{s}}}$ (MeV)						
(MeV/c^2)	2.58	3.58	4.58	5.58	6.58	7.58	8.58
4801	14.5/8.5/16.2	14.1/8.5/20.7	13.4/10.8/20.4	14.1/10.7/23.7	10.3/10.9/23.8	11.5/11.7/23.2	11.1/12.7/24.1
4806	14.5/6.1/21.2	14.2/6.2/18.3	13.5/8.3/17.3	14.1/7.7/18.2	14.0/10.4/18.3	15.5/12.6/17.8	11.1/13.6/23.7
4811	14.5/3.8/21.0	14.2/6.3/20.2	13.5/7.8/19.9	14.1/7.8/20.9	26.2/10.4/23.2	23.7/12.7/22.6	23.0/13.9/23.4
4816	14.1/4.7/16.3	13.8/6.8/20.8	24.6/6.6/26.3	25.8/9.1/27.6	25.6/9.5/27.8	28.3/12.4/23.3	27.5/13.0/24.2
4821	25.8/6.7/16.9	25.2/7.5/16.2	24.1/7.5/21.2	25.1/9.0/22.3	24.9/9.2/19.3	27.6/9.5/30.2	26.8/11.0/31.4
4826	26.4/8.6/16.4	25.8/9.3/15.8	24.6/9.1/15.6	25.7/9.1/18.6	25.5/10.2/18.7	28.3/11.2/23.4	27.5/11.4/24.3
4831	27.1/7.0/21.1	26.5/8.6/20.3	25.2/11.0/20.1	26.4/11.2/21.0	34.7/11.5/23.4	38.5/12.0/22.8	37.4/12.5/23.6
4836	13.8/6.6/16.2	13.5/7.5/15.6	32.0/9.7/23.3	33.4/9.4/23.7	33.1/9.6/23.8	36.6/12.2/23.2	35.6/13.8/24.1
4841	24.7/6.9/21.9	24.2/6.7/18.1	23.1/7.2/17.9	24.1/8.9/18.8	23.9/9.9/24.3	34.9/12.0/29.6	34.0/13.4/30.8

$|1-\Pi|^2$ are 0.931, 0.930, and 0.929 for $\sqrt{s} = 10.52$, 10.58, and 10.867 GeV [31], and the uncertainty is calculated to be less than 0.1%, which is negligible. The radiative correction factors $(1+\delta)_{\text{ISR}}$ are 0.686, 0.694, and 0.738, as calculated using the formula given in Ref. [32] for $\sqrt{s} = 10.52$, 10.58, and 10.867 GeV, respectively, where we assume that the dependence of cross sections on s is $1/s$.

The calculated 90% CL upper limits on the product branching fractions of $\Upsilon(1S, 2S) \to X_{cc\bar{s}\bar{s}} + \text{anything}$ and the product values of Born cross section and branching fraction of $e^+e^- \to X_{cc\bar{s}\bar{s}} + \text{anything}$ at $\sqrt{s} = 10.52$, 10.58, and 10.867 GeV for the mode $X_{cc\bar{s}\bar{s}} \to D_s^+D_s^+$ ($X_{cc\bar{s}\bar{s}} \to D_s^{*+}D_s^{*+}$) are displayed in Fig. 6 (7). Numerical values for the mode $X_{cc\bar{s}\bar{s}} \to D_s^+D_s^+$ can be found in Tables III and IV, while those for the mode $X_{cc\bar{s}\bar{s}} \to D_s^{*+}D_s^{*+}$ are shown in Tables V and VI.

VII. CONCLUSION

Using the data samples of 102×10^6 $\Upsilon(1S)$ events, 158×10^6 $\Upsilon(2S)$ events, and data samples at $\sqrt{s} = 10.52$, 10.58, and 10.867 GeV corresponding to integrated luminosities 89.5, 711.0, and 121.4 fb^{-1}, respectively, we search for the double-heavy tetraquark states $X_{cc\bar{s}\bar{s}}$ in the processes of $\Upsilon(1S, 2S) \to D_s^+D_s^+(D_s^{*+}D_s^{*+}) + \text{anything}$ and $e^+e^- \to D_s^+D_s^+(D_s^{*+}D_s^{*+}) + \text{anything}$ at $\sqrt{s} = 10.52$, 10.58, and 10.867 GeV. No peaking structures are observed in the $M_{D_s^+D_s^+}$ and $M_{D_s^{*+}D_s^{*+}}$ distributions from data. The 90% CL upper limits on the product branching fractions in $\Upsilon(1S, 2S)$ inclusive decays $[\mathcal{B}(\Upsilon(1S, 2S) \to X_{cc\bar{s}\bar{s}} + \text{anything}) \times \mathcal{B}(X_{cc\bar{s}\bar{s}} \to D_s^+D_s^+(D_s^{*+}D_s^{*+}))]$ and the product values of Born cross section and branching fraction for $e^+e^- \to X_{cc\bar{s}\bar{s}} + \text{anything}$ $[\sigma(e^+e^- \to X_{cc\bar{s}\bar{s}} + \text{anything}) \times \mathcal{B}(X_{cc\bar{s}\bar{s}} \to D_s^+D_s^+(D_s^{*+}D_s^{*+}))]$ at $\sqrt{s} = 10.52$, 10.58, and 10.867 GeV as functions of various assumed $X_{cc\bar{s}\bar{s}}$ masses and widths are determined.

ACKNOWLEDGMENTS

We thank the KEKB group for the excellent operation of the accelerator; the KEK cryogenics group for the efficient operation of the solenoid; and the KEK computer group, and the Pacific Northwest National Laboratory (PNNL) Environmental Molecular Sciences Laboratory (EMSL) computing group for strong computing support; and the National Institute of Informatics, and Science Information NETwork 5 (SINET5) for valuable network support. We acknowledge support from the Ministry of Education, Culture, Sports, Science, and Technology (MEXT) of Japan, the Japan Society for the Promotion of Science (JSPS), and the Tau-Lepton Physics Research Center of Nagoya University; the Australian Research Council including Grants No. DP180102629, No. DP170102389, No. DP170102204, No. DP150103061, and No. FT130100303; Austrian Federal Ministry of Education, Science and Research (FWF) and FWF Austrian Science Fund No. P 31361-N36; the National Natural Science Foundation of China under Contracts No. 11675166, No. 11705209, No. 11975076, No. 12135005, No. 12175041, and No. 12161141008; Key Research Program of Frontier Sciences, Chinese Academy of Sciences (CAS), Grant No. QYZDJ-SSW-SLH011; the Shanghai Science and Technology Committee (STCSM) under Grant No. 19ZR1403000; the Ministry of Education, Youth and Sports of the Czech Republic under Contract No. LTT17020; Horizon 2020 ERC Advanced Grant No. 884719 and ERC Starting Grant No. 947006 "InterLeptons" (European Union); the Carl Zeiss Foundation, the Deutsche Forschungsgemeinschaft, the Excellence Cluster Universe, and the VolkswagenStiftung; the Department of Atomic Energy (Project Identification No. RTI 4002) and the Department of Science and Technology of India; the Istituto Nazionale di Fisica Nucleare of Italy; National Research Foundation (NRF) of Korea Grants No. 2016R1D1A1B01010135,

No. 2016R1D1A1B02012900, No. 2018R1A2B3003643, No. 2018R1A6A1A06024970, No. 2019K1A3A7A09033840, No. 2019R1I1A3A01058933, No. 2021R1A6A1A03043957, No. 2021R1F1A1060423, and No. 2021R1F1A1064008; Radiation Science Research Institute, Foreign Large-size Research Facility Application Supporting project, the Global Science Experimental Data Hub Center of the Korea Institute of Science and Technology Information and KREONET/GLORIAD; the Polish Ministry of Science and Higher Education and the National Science Center; the Ministry of Science and Higher Education of the Russian Federation, Agreement No. 14.W03.31.0026, and the HSE University Basic Research Program, Moscow; University of Tabuk research Grants No. S-1440-0321, No. S-0256-1438, and No. S-0280-1439 (Saudi Arabia); the Slovenian Research Agency Grants No. J1-9124 and No. P1-0135; Ikerbasque, Basque Foundation for Science, Spain; the Swiss National Science Foundation; the Ministry of Education and the Ministry of Science and Technology of Taiwan; and the United States Department of Energy and the National Science Foundation.

[1] M. Gell-Mann, Phys. Lett. **8**, 214 (1964).
[2] S. K. Choi *et al.* (Belle Collaboration), Phys. Rev. Lett. **91**, 262001 (2003).
[3] D. Acosta *et al.* (CDF Collaboration), Phys. Rev. Lett. **93**, 072001 (2004).
[4] V. M. Abazov *et al.* (D0 Collaboration), Phys. Rev. Lett. **93**, 162002 (2004).
[5] B. Aubert *et al.* (*BABAR* Collaboration), Phys. Rev. D **71**, 071103 (2005).
[6] E. S. Swanson, Phys. Lett. B **588**, 189 (2004).
[7] C. Y. Wong, Phys. Rev. C **69**, 055202 (2004).
[8] N. Li and S. L. Zhu, Phys. Rev. D **86**, 074022 (2012).
[9] L. Maiani, F. Piccinini, A. D. Polosa, and V. Riquer, Phys. Rev. D **71**, 014028 (2005).
[10] K. K. Seth, Phys. Lett. B **612**, 1 (2005).
[11] C. Z. Yuan, Int. J. Mod. Phys. A **33**, 1830018 (2018).
[12] N. Brambilla, S. Eidelman, C. Hanhart, A. Nefediev, C. P. Shen, C. E. Thomas, A. Vairo, and C. Z. Yuan, Phys. Rep. **873**, 1 (2020).
[13] R. Aaij *et al.* (LHCb Collaboration), arXiv:2109.01038.
[14] R. Aaij *et al.* (LHCb Collaboration), arXiv:2109.01056.
[15] S. S. Agaev, K. Azizi, and H. Sundu, Phys. Rev. D **99**, 114016 (2019).
[16] C. E. Fontoura, G. Krein, A. Valcarce, and J. Vijande, Phys. Rev. D **99**, 094037 (2019).
[17] G. Yang, J. L. Ping, and J. Segovia, Phys. Rev. D **101**, 014001 (2020).
[18] L. Leskovec, S. Meinel, M. Pflaumer, and M. Wagner, Phys. Rev. D **100**, 014503 (2019).
[19] G. Yang, J. L. Ping, and J. Segovia, Phys. Rev. D **102**, 054023 (2020).
[20] A. Abashian *et al.* (Belle Collaboration), Nucl. Instrum. Methods Phys. Res., Sect. A **479**, 117 (2002); also, see detector section in J. Brodzicka *et al.*, Prog. Theor. Exp. Phys. **2012**, 04D001 (2012).
[21] S. Kurokawa and E. Kikutani, Nucl. Instrum. Methods Phys. Res., Sect. A **499**, 1 (2003), and other papers included in this volume; T. Abe *et al.*, Prog. Theor. Exp. Phys. **2013**, 03A001 (2013), and references therein.
[22] D. J. Lange, Nucl. Instrum. Methods Phys. Res., Sect. A **462**, 152 (2001).
[23] R. Brun *et al.*, GEANT 3: User's guide Geant 3.10, Geant 3.11, CERN Report No. DD/EE/84-1, 1984, https://inspirehep.net/literature/252007.
[24] R. E. Mitchell *et al.* (CLEO Collaboration), Phys. Rev. D **79**, 072008 (2009).
[25] E. Nakano, Nucl. Instrum. Methods Phys. Res., Sect. A **494**, 402 (2002).
[26] G. Punzi, *Proceedings of the PHYSTAT 2003* (Stanford, USA, 2003), p. MODT002, https://www.slac.stanford.edu/econf/C030908/papers/SLAC-R-703.pdf.
[27] P. A. Zyla *et al.* (Particle Data Group), Prog. Theor. Exp. Phys. **2020**, 083C01 (2020).
[28] X. Y. Zhou, S. X. Du, G. Li, and C. P. Shen, Comput. Phys. Commun. **258**, 107540 (2021).
[29] G. J. Feldman and R. D. Cousins, Phys. Rev. D **57**, 3873 (1998).
[30] J. Conrad, O. Botner, A. Hallgren, and C. Pérez de los Heros, Phys. Rev. D **67**, 012002 (2003).
[31] S. Actis *et al.*, Eur. Phys. J. C **66**, 585 (2010).
[32] E. A. Kuraev and V. S. Fadin, Yad. Fiz. **41**, 733 (1985); [Sov. J. Nucl. Phys. **41**, 466 (1985)].